Supplementary Materials for

The quandary of detecting the signature of Climate change in Antarctica

M. Casado*, R. Hébert, D. Faranda , A. Landais

*Corresponding author. Email: mathieu.casado@gmail.com

This PDF file includes:

Supplementary text S1 to S8
Figures S1 to S4
Tables S1 to S6
References (1 to 48)

Supplementary Text

1. Antarctic climate reconstructions

The stack method used in this manuscript (see Methods) is very simple in the sense that records are averaged to the stack when available, leading to a variable numbers of records, and that no adjustment of the variance or weight is applied to these records, as opposed to the stack published in Stenni et al(Stenni et al., 2017) (hereafter S17). This methodology was applied to be comparable with the results obtained from the persistence, which is calculated on independent records and averaged together with no weight. In this section, we compare the outputs of our stack method and of the outputs of (Stenni et al., 2017) to evaluate the impact of the stacking.

We produce time series of isotopic composition variations over the last 1000 years for each region described in S17 following the same *simple-stacking* methodology than described in the Methods section of the main text. We plot these 1000-year time series together with two stacks produced in S17: the unweighted stack (purple lines in all subplots of Figure ED5) and the CPS stack (yellow lines). The regional time series, as well as the Pan-Antarctic stack, show relatively similar variability than the reconstructions previously in S17 (Figure ED5 and Table S1). For the CPS reconstruction, annual stacks were available for each region and for all of Antarctica, so the correlations were realised with annual data, including all the impact of inter-annual variability which is for most of the cores including archival noise (Fig. ED5). For the unweighted stacks, only decadal averages were available and so the correlations are limited to decadal and centennial variability. In most cases, relatively good correlations are obtained with r values superior to 0.5. In some cases, the difference of the weight of individual cores from the CPS methods and the stack provided here lead to weaker correlation. For instance, for the East Antarctica and Antarctica regions, the correlations between the CPS time series and our stack are relatively low (around 0.5) due to the relatively high weight of the Plateau Remote core in the CPS reconstruction with an extreme positive anomaly (~4‰) 1000 years ago (Supplementary figure S4 of S17). In general, the differences between our stack (which is unweighted) and the unweighted stack from S17, comes from the fact that we average the annually resolved cores before preparing block averages to decadal resolution while they first interpolated to decadal resolution before averaging the cores together.

Table S1: *Correlation (r values) between the stack time series produced here and the CPS and the unweighted reconstructions produced S17* (Stenni et al., 2017)

Region	Last 1000 years		Last 200 years	
	CPS	Unweighted	CPS	Unweighted
East Antarctica	0.65	0.84	0.82	0.61
Indian Coast	0.90	0.85	0.61	0.94
Weddel Coast	1	0.90	1	0.89
Antarctic Peninsula	0.92	0.88	0.85	0.88
West Antarctica	0.67	0.80	0.88	0.76
Victoria Land	0.73	0.92	0.79	0.81
DML Coast	0.70	0.83	0.70	0.65
Antarctica	0.54	NA	0.69	NA

$p < 0.05$ for all correlations

The time series overall show relatively good agreement, both for all of Antarctica (Figure 1 and Figure S1g), and regionally (Figure ED5), in particular with the unweighted stack of Stenni et al. Moving trends applied to all three stacks also show similar results, in line with Stenni et al, that a significant warming trend in the context of the last 1000 years is not obvious (Fig. 1 and ED5).

2. Signal to noise ratio

In order to resolve the relative contribution to the ice core records of the climatic signal, and thus identify the timescale at which a significant climatic signal can be detected in the isotope record, we calculate the Signal to Noise Ratio (SNR), i.e. the amount of common climatic signal archived in the ice core records compared to the decorrelated archival noise.

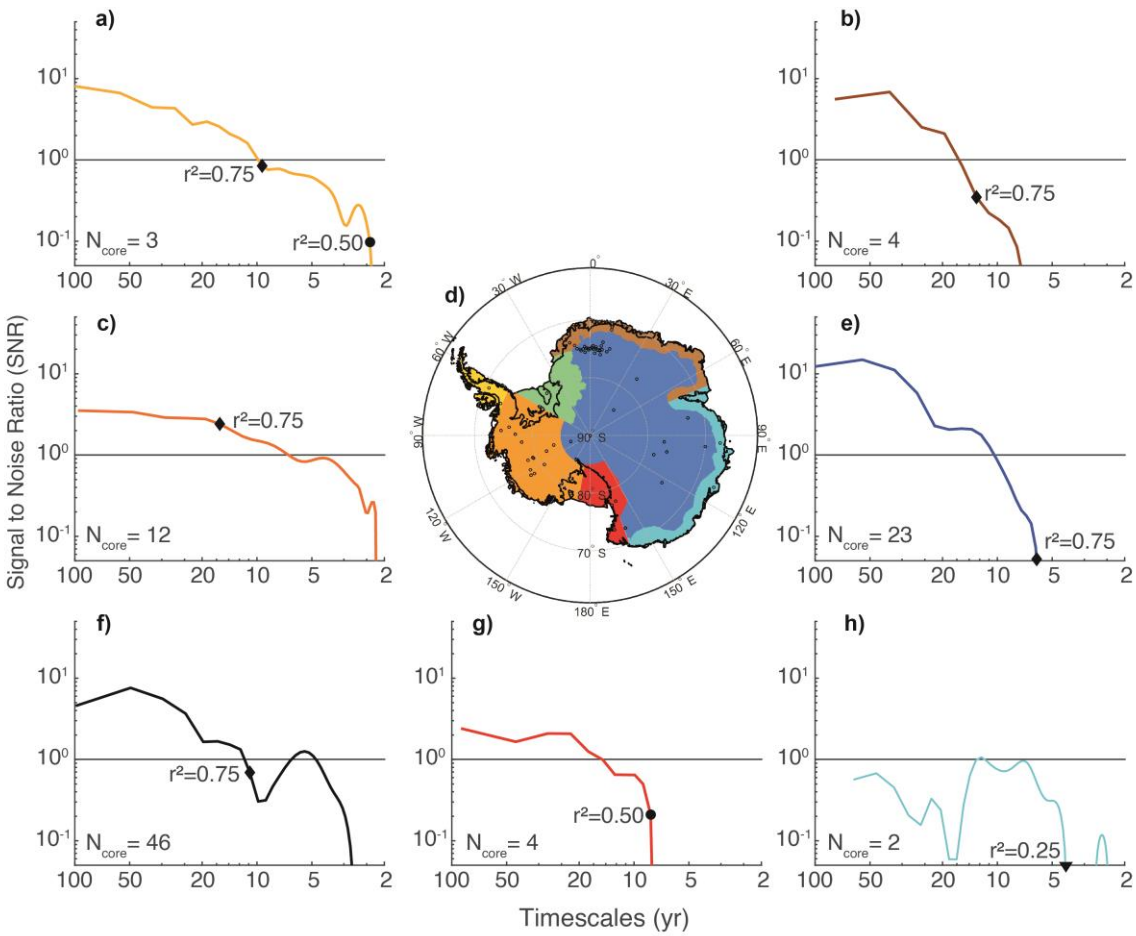

***Figure S1**: Spectral analyses of the signal to noise ratio for the isotopic composition of ice cores of each regions where more than one core was available: a) Antarctic Peninsula, b) Dronning Maud Land Coast, c) West Antarctica, e) East Antarctic Plateau, f) all of Antarctica, g) Victoria Land, and h) Indian Coast. The map of all the ice cores in the different regions is shown in the central block (d). The correlation coefficient (r^2) corresponds to the theoretical correlation between the stack made with these records and the common climatic signal for this given SNR* (Münch and Laepple, 2018).

The SNR is computed by comparing the power spectral density (PSD) of individual records with the PSD of their average. We estimate the power spectral density (PSD) from each individual record using Thomson's multitaper spectral estimate (Percival and Walden, 1993), and calculate the SNR as a function of timescale for the individual regions where more than one record is available following the calculation from (Münch and Laepple, 2018), and for the whole continent (Fig. S1).

Overall, identifying the signature of climate change on the temperature in Antarctica has been hampered by the rather large amplitude of natural variability at interannual and decadal scales compared to the amplitude of climate change (Clem et al., 2020). In ice core records, an additional archival noise is overlayed on these two signals (Casado et al., 2018; Laepple et al., 2018), leading to limited trust in the recorded signal at scales ranging from interannual to centennial (Casado et al., 2020). These archival noises being only locally coherent, it can be averaged out by combining a large number of ice cores far enough from one another. In this way, we extract the common climatic signal for a region, and separate within the ice core records (i) the climatic signal (both natural and forced variability) and (ii) the archival noises.

For a single region, the individual spectra include (i) a common climatic signal and (ii) an incoherent noise linked with archival processes. The mean spectrum of all individual spectra include the mean power associated with both the climatic signal and the archival noise. The mean spectrum divided by the number of records is the expected spectrum if all isotopic variations present in the ice core record were independent noise (since incoherent noise averages out with a factor 1/N). In comparison, when averaging all the records in the time domain, the noise component is still divided by the factor 1/N, but the common climatic signal is not altered (Münch and Laepple, 2018). A signal to noise ratio larger than 1 is thus obtained for timescales between 10 and 20 years for all regions in Antarctica except the Indian Coast (Fig. S1). These high SNR values (Christiansen and Ljungqvist, 2017) indicate that the regional stack correlates with the common temperature signal (see Methods from (Münch and Laepple, 2018)) with values ranging from $r^2 = 0.25$ for the Indian Coast region at timescales longer than 3 years, to $r^2=0.50$ for Victoria Land regions for timescales longer than 8 years, to $r^2=0.75$ for West Antarctica, the Antarctic Peninsula, East Antarctic Plateau, and all of Antarctica, for timescales longer than 10 years.

This analysis only presents the total SNR for the isotopic signal in the ice core records, and cannot discriminate if the signal is linked with (i) anthropogenic warming or (ii) natural variability. However, the relatively high SNR found across the different regions, due partly to the large number of cores, show that a meaningful climatic signal can be extracted from decadal scale for all regions except Indian Coast and the Weddel Coast regions. The SNR estimates were performed on a subset of the cores covering the largest common period for each region (windows covering the last 100 to 150 years only of the records) since a constant number of cores is required to compute the stack. As a result, this means that the SNR presented here is thus an upper bound value for the SNR of the full stacks including in general the most recent period, with the largest number of cores, which is fortunately concomitant with the period of anthropogenic warming. Since the anthropogenic warming signal induces mainly a decadal to multi-decadal signal (Clem et al., 2020), the SNR evaluation suggests that using both regional and pan-Antarctic stacks of ice core records is relevant to study decadal to centennial variability in the context of the last 150 and 1000 years, respectively (Von Storch et al., 2004). Yet, due to the similar amplitude of the contribution of internal variability and warming trend (Goosse et al., 2005), traditional statistical analysis could still fail to detect the impact of very present anthropogenic climate change (Stenni et al., 2017).

3. Detecting the Anthropogenic climate change in presence of natural variability

Detecting a trend in a noisy signal requires a large number of datapoints, so the signal to noise ratio becomes high enough so the linear regression can accurately evaluate the trend. In the case of the climate system, the detection of the anthropogenic climate change in natural archives requires to disentangle the trend from the climatic time series which includes not only archival noises (usually a white noise (Casado et al., 2020; Laepple et al., 2018)), but also natural variability with a characteristic positive autocorrelation (akin to red noise) (Zhu et al., 2019). Such signal tends to hinder the ability to detect a regime shift efficiently (Rodionov, 2006) due to more persistent anomalies at longer time scales than at short times scales. This can directly affect the accuracy of the calculation of a running trend, especially if the amplitude of the natural variability is of the same order of magnitude than the trend over similar time scales. In this section, we illustrate this effect for three different cases: (1) a combination of white noise and a trend of varying amplitude, (2) a combination of white noise, a common red signal of fixed amplitude, and a trend of varying amplitude, and (3) a combination of white noise, a common red signal of varying amplitude, and a trend of fixed amplitude. In these three cases, we simulate 1000 runs for which we compute the trend over a 40-year window and the persistence (see methods), and calculate the time series. We compare these time series to the pan-Antarctic stack of δ^{18}O records using the relation $\delta^{18}O \approx 0.5 \times T$. While isotope-temperature relationship will change the amplitude of the climate change, as discussed in the Methods, here, since the archival noise and the natural variability will be scaled with the same factor, it does not change the outcome. We arbitrarily fixed the date of the start of the warming trend to 1880 for illustration purposes, even though the imprint of anthropogenic climate change in Antarctica is unlikely to be visible so early.

First, we simulate the case of the combination of a white noise and a trend of varying amplitude, which is equivalent to a climatic system in which the natural variability is very small compared to both the archival noise and the anthropogenic climate trend, an obviously unrealistic situation. The results are presented in Fig. ED2. Since we present the average of 1000 iterations, the white noise is completely averaged out, and we observe a very linear response of δ^{18}O at odds with the observations. The 40-year running trend increases linearly between 1880 and 1920, and then reach a constant value, as expected. For the persistence, we applied an offset of +0.09 yr^{-1} to the value of Θ to make the comparison with the observations easier (red noise, as well as impact of isotopic diffusion (Gkinis et al., 2021) explain this offset, evaluated from computing the persistence on raw and diffused white noise simulated for all the core locations included in this manuscript, using the proxy forward model described in (Casado et al., 2020)). We observe an increase in Θ over the course of roughly 100 years, before it stabilises to a higher value. Since Θ describes the residence time around a given climate state, a larger trend leads to higher values of the persistence as the system remains more time at a given temperature level away from the equilibrium position. The observed change of persistence and δ^{18}O seems to suggest different average values of the trend induced by the anthropogenic climate change. Indeed, we observe in the pan-Antarctic stack an increase in the mean value of Θ of roughly 0.026 y, best approximated in this simple case by a warming of 0.1°C/dec. On the other hand, the trend from the time serie itself matches the best with warming between 0.12 and 0.2°C/dec. In addition, the transition time from low to high Θ seems to occur faster in the observations than in the simulations. This simple case illustrates the effect of noise to evaluate a trend and its associated impact on persistence, but fails to represent the complex system that we are facing here.

Second, we evaluate the impact of natural variability to the calculation of the trend in a noisy signal. To do so, we generate a common climatic signal for the 1000 iterations with a scaling of $\beta = 0.6$, as suggested for Antarctica (Casado et al., 2020; Münch and Laepple, 2018), and to which we add a randomly generated white noise and a trend from 1880. This simulated common climatic signal is generated to have roughly the same amount of power at the decadal scale (0.52‰²/yr on average over the frequency band from 1/10 to 1/40 yr^{-1}) than the observations (0.59‰²/yr). The results are presented in Fig. ED3. Since the common climatic signal is simulated randomly, even though it is the same for the 1000 iterations, the phase is not matching with the phase of the observations and as a result, we do not expect a good agreement between the simulated and observed time series. Nonetheless, the change of persistence and the imprinted trends should share similar evolutions, and we will try to assess here what are the effects of the natural variability on the detection of the trend. Similarly to the first case, we observe that for increasing warming trend, the persistence response gets larger. Yet, for the same amplitude of warming, the amplitude of persistence change is reduced compared to the case without any natural variability. With natural variability, the warming trend which matches best the change of persistence is now 0.2°C/dec, in line with the observations (see Fig. 3 in the main text). The simulated moving trend obtained with the combination of a warming signal and natural variability shares also properties of the moving trend realised on the observations, with oscillatory behaviour resulting to variable trends. This shows the limitation of the moving trend in the case of signal containing a red component (or more generally, when the natural variability at decadal scale is of a similar amplitude than the forced variability). It also appears obvious than the trend imposed to start in 1880 is not a realistic solution since the change of $\delta^{18}O$ occurs too early compared to the observations, leading to overestimation of the values by the year 2000. We nonetheless decide to keep this startdate as it gives a long enough period for our simulations to lead to a stabilised value of persistence and of the running trends (a full strength temperature increase starting in the 1950s would not provide a time span long enough to see the system unfold). Overall, the simultaneous change of trend and persistence is here the key aspect to evaluate the amplitude of the observed climate change. Indeed, we show here that the calculation of the trend alone is affected by the start and end date (or start date and length of the window over which the trend is calculated), and the amplitude of the trend compared to the natural variability and the archival noise.

Third, we evaluate the impact of a varying natural variability (Fig. ED4) on the observed trends and change of persistence. We fix the warming trend at a value of 0.2°C/dec, in line with the observations (see Fig. 3 of the main text). The natural variability is still modelled with a scaling of $\beta = 0.6$. In this case, the moving trends have globally the same average values, but with larger natural variability, excursions around the means are amplified, leading to an increasing difficulty to interpret its value. For larger value of natural variability, the change of persistence Θ is decreased. This can be interpreted as the amplitude of the trend becoming not large enough for the system to be changing, and thus residing in the same state. In this case, we observe that the change of perspective is quite sensitive to the amount of natural variability, and here, that a value 0.7 and 1.4°C²/yr would fit best the observations. Similar tests change the scaling of the natural variability (Huybers and Curry, 2006; Lovejoy and Schertzer, 2013) indicate a similar influence on the changes of persistence: by changing the distribution of power spectral density and adding more variability at larger time scales, the changes induced by the trend here at the decadal time scales become more important compared to the natural variability, and thus for larger values of β, we observe larger changes of Θ (not shown). We have shown here that the persistence is a complementary metric to a classical trend for signals where a warming is convoluted with natural variability since it can help evaluate the amplitude of trend to the natural variability.

4. MonteCarlo simulation of the relative amplitude of the present climate change and natural variability in Antarctica

We propose to use the observations of change of persistence and trend between 1950 and 2005 to evaluate the actual amplitude of the climate change in comparison with the natural variability. As described in the previous section, we identified three parameters which affect the persistence and the moving trend: the amplitude of the warming trend, the mean decadal variability, and the scaling of the common climatic signal. It might sound paradoxical that the measured trend is not used directly, but only used as an observable helping to evaluate the actual warming trend, indeed, as shown in the Extended Data Section 2, the measured trend is strongly affected by the natural variability and thus can lead to gross uncertainties on the evaluation of the actual warming. Here, we suggest that by combining it with the persistence, the value can be validated.

We realise a monte carlo simulation randomly picking the mean decadal natural variability amount (NV), the scaling of the natural variability (β) and the warming trend amplitude (trend) and compute the predicted change of persistence ($\Delta\Theta$) and the simulated trend between 1950 and 2005 ($trend_s$). Each iteration covers 1800 to 2000, with average of 50 individual "virtual cores" (roughly the same number than the pan Antarctic stack for this period) including common natural variability (Y, simulated with a power law of β so that the average amount of natural variability over the timescales ranging from 10 to 40 years has a given value NV), independent white noise, and common trend (randomly chosen for each iteration with an amplitude trend, see Table S2).

Table S2: *Range of accepted parameters for the monte carlo simulation*

Parameter	Range of simulated values	Values from the literature
β	0 – 1	0.6 (Münch and Laepple, 2018)
NV (‰^{2} yr^{-1})	0 – 4.5	-
Trend (‰ dec^{-1})	0 – 0.5 (~ 0 – 1°C dec^{-1})	0.6°C dec^{-1} (Clem et al., 2020)

We make use of the predicted values of $\Delta\Theta$ to compute an error (RMSE) variable associated with each iteration of the Monte Carlo simulation, using the observed changes of persistence ($\Delta\Theta_{obs}$ = 0.026 yr). We present the ensemble of values of mean decadal natural variability amount (NV), the scaling of the natural variability (β) and the warming trend amplitude (trend) which minimise this error in Fig. S2. The consecutive envelopes represent the distribution of obtained values of the input parameter different threshold of error (from 0.05 to 0.005) and indicates that the distribution remains coherent regardless of the threshold put for the error. This provides us with a range of values β, NV and the trend of 0.44±0.30, 0.6±0.4‰^{2} y, and 0.16±0.03‰ dec^{-1}, respectively. The error bars are relatively large, in particular for the variability which has only a weak constrain on the persistence change compared to the trend (the slope of the surface in Fig. 1b) is steeper for the trend than for the natural variability). Independent calculation of the decadal variability on the dataset suggests values of 0.52 and 0.64 ‰^{2} y for β and NV, respectively. The constrain on β and NV remains rather loose since both parameters tend to counteract one another signature on the persistence change $\Delta\Theta$. Nonetheless, the trend necessary to create observed changes of persistence has a relatively narrow error bar, in line with traditional trend estimates.

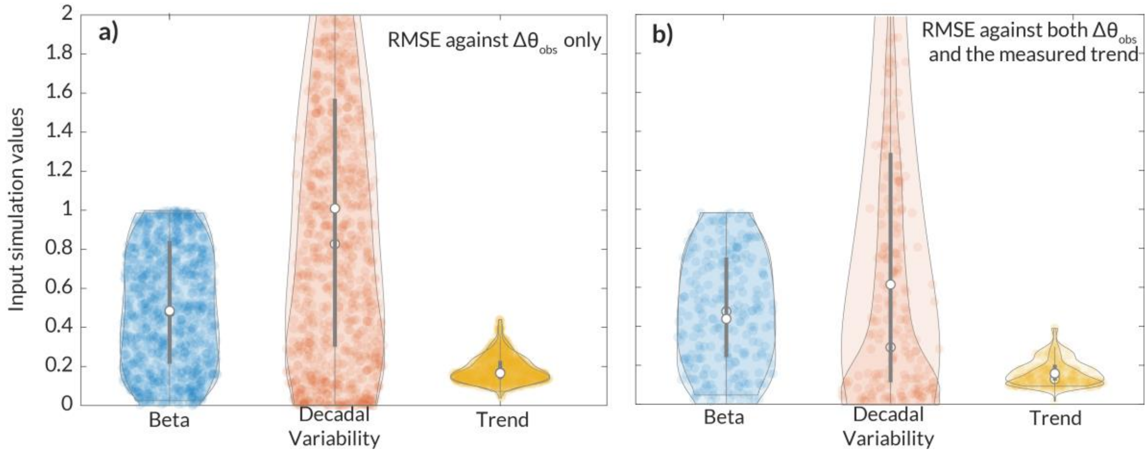

Figure S2: *Outputs of the monte carlo simulation for the observed changes of persistence and trend in a noisy system as a function of the spectral characteristics of the natural variability (modelled with a red noise with different values of β and average decadal variability values) and the impact of a trend of a given amplitude.*

If we calculate the error variable using both $\Delta\Theta_{obs}$ and the observed trend, we obtained similar values of the predicted warming trend of 0.16±0.04‰ dec^{-1}. These results indicate that the persistence is sufficient here to prescribe the value of the trend that generated the observed warming in Antarctica, and validate that a significant warming trend associated with the anthropogenic climate change is present in the ice core data in Antarctica in a way that was unprecedented in the context of the last 1000 years, despite moving trend of the same amplitude than the one observed in the last 50 years being already seen in the past due to the strong decadal variability.

We use these results to create a conversion scale between the observed change of persistence and the trend needed to generate such a change. This conversion provides for each region a value of the changes of ‰ dec^{-1} equivalent to the change of persistence (Table S3). By including isotope to temperature conversion, we use these results to include a second y-axis in Figure 3b in the main text.

5. Impact of the window length on trend estimates

In this section, we delve into the difference of trends obtained here, and in Stenni et al, (Stenni et al., 2017). We showed in Section S1 of the Supplementary Materials that the stacks are very similar, and in particular that the stacking method does not influence on the trend estimates. We evaluate the impact of the length of the window used for the trend estimates. Indeed, while our conclusions differ from Stenni et al (Stenni et al., 2017), we argue that the results presented here are actually in agreement with the ones used in Stenni et al, but that the choice of the windows used to estimate the trend imprinted by the current climate change was not appropriate. Calculating a trend in a noisy challenge is challenging because for a window too short, the noise creates significant uncertainties on estimate of the trend, and for a window too long, the accuracy of the trend is reduced because the window encompasses a period where the climate was not warming at the same pace (or not at all).

To illustrate the impact of the window length, we calculate the trends for increasing window length, with a fixed end date in 2005 when the number of records drop (so the beginning of the window used to compute the trend is equal to 2005 – Window Length) for both our stack record and in the CPS time serie produced in Stenni et al (Fig ED1, black and purple curves respectively). For windows shorter than 30 years, both series include significant uncertainty due to decadal variability hiding the actual warming signal. Between 30 and 70 years, we observed a more stable regime where the average value correspond to the actual trend value, here, for both time series, around 0.11‰/dec, equivalent to around 0.22°C/dec (Methods). For windows longer than 70 years, the obtained trends decrease rapidly because the time series include both period affected and not affected by climate change, which, in Antarctica is suspected to start to be visible around 1980 (Abram et al., 2016).

We simulated the impact of both these effects (competition of the decadal variability for small window length and dilution of the trend for long window length) for arbitrary conditions analogous to the ones expected in Antarctica: similarly to Section S3, we generated times series with a β of 0.6, decadal natural variability at a level of 0.6‰ y^{-1}, and with a fixed trend of 0.1‰/dec starting 50 years before the end of the time series. We simulate 50 synthetic signals (similar number than for the Antarctic stack) and average out the trends for increasing window length. We obtain a very good match with the observations (Green line in Fig. ED1), illustrating numerically with a pseudo-proxy experiment the issues with window length to estimate trends for noisy signals. In Stenni et al, (Stenni et al., 2017), by using windows of 100 years, while less than 50% of the window was probably under the influence of the anthropogenic warming, the obtained trends were under-estimated two to three folds the actual warming. By plotting the obtained trends against with window length, we propose a diagnostic to retrieve a better estimate of the actual trend without cherry picking the length to obtain the best results. To evaluate the error made in the trend estimator in the case of a given number of cores N for a given region (for instance, for the Antarctic stack, N = 50), we use 10 000 iterations of the simulation to evaluate the confidence interval and scale the value by $\sqrt{N}$ (green shade in Figure ED1).

Table S3: *"Best guesses" of the trends induced by climate change in the time series for each regions for the stack from this study, the CPS stack* (Stenni et al., 2017)*, and suggested by the persistence changes for conversion (Section S3).*

Region	Window (years)	Uncertainty for 50yr window (‰/dec)	Slope (‰/dec)		
			This Study trend	CPS Stenni et al, 2017 trend	Persistence method
East Antarctica	50-65	±0.04	0.10	0.098	0.18
Indian Coast	NA	±0.12	NA	NA	0.09
Weddel Coast	NA	±0.17	NA	NA	0.19
Antarctic Peninsula	40-60	±0.08	0.19	0.28	NA
West Antarctica	40-60	±0.05	0.24	0.22	0.14
Victoria Land	NA	±0.08	NA	NA	0.15
DML Coast	40-60	±0.08	0.34	0.17	NA
All Antarctica	35-45	±0.02	0.11	0.10	0.16

We use the trends estimate as a function of the window length to evaluate the best window span over which realise the trend to minimise both the uncertainty associated with the competition with the decadal variability and the dilution of the trend for long windows, and obtain the best guess of the actual trend present in the records. We apply this method for the time series of each region, both for our ice core stack and for the CPS reconstruction (Stenni et al., 2017) (Table S3). For East Antarctica, West Antarctica and all of Antarctica, we obtain very good agreement between our stack and the CPS reconstruction. For the Antarctic Peninsula and DML Coast, where a small number of cores amplifies the impact of the different weight applied in the stacking methods, we obtain relatively different results. Interestingly, for both these regions, the increases of persistence were too small to evaluate a significant impact of a trend, suggesting that the internal variability impact was largely dominating (Section S2). For East Antarctica, West Antarctica, and All of Antarctica, the persistence method is still at odds with the traditional trend estimates, which could mean that the windows were still too short to remove the competition with the natural variability, but the dilution of the trend for long window length prevents from testing the hypothesis.

6. Isotope to Temperature relationship

Calibrating isotopic data into temperature is complex, as illustrated by the large amount of literature about it (Casado et al., 2013; Osborn and Briffa, 2004). In particular, biases can occur when the calibration is done on the recent period only at high frequencies if the proxy records include a large amount of archival noise. In this context, independent slopes, either from spatial relationship (Masson-Delmotte et al., 2008), observed in precipitation samples (Touzeau et al., 2016), from isotope-enabled models (Werner et al., 2018), or from the use of isotopic composition of inert gases such as $\delta^{40}Ar$ or $\delta^{15}N$ (Guillevic et al., 2013) provide a safer alternative to evaluate the right amount of variance at the decadal scale, but the calibration is then potentially limited to a short range of climatic conditions and time scales. Here we suggest to use the average value of the $\Delta\delta^{18}O/\Delta T$ slopes observed in precipitation in Antarctica (~0.5‰.°C^{-1}) (Casado et al., 2017) and to include the range of values found in the literature as an error bar (from ~0.3 to 0.8‰.°C^{-1}, see Table S4). They cover a relatively large range of values in line with other observations from other type of studies, for instance looking at the surface snow isotopic composition variations either spatially (Landais et al., 2017; Masson-Delmotte et al., 2008) or temporally (Casado et al., 2018; Küttel et al., 2012).

Table S4: *Slope $\Delta\delta^{18}O/\Delta T$ found in precipitation in Antarctica*

Site	Slope $\Delta\delta^{18}O/\Delta T$ (‰.°C^{-1})	Reference
Vostok	0.26 – 0.35	Landais et al, 2012, Touzeau et al, 2016
Dome C	0.45	Stenni et al, 2016
Dome F	0.76	Fujita et al, 2006
Neumayer	0.57	Schlosser et al, 2004

The range of calibration between isotopic composition and temperature can be refined thanks to the spectral comparison between temperature records and ice core data. Since we average a large number of ice core records in our stack, the contribution of the archival noises in the spectrum is very limited, hence limiting the biases induced by the calibration (Osborn and Briffa, 2004). In the manuscript, we compared the ice core stacks to ERA5 gridded temperature data at the ice core location. There are known biases present in ERA5, in particular, a discontinuity at the beginning of the satellite era in 1979. We test alternative temperature reconstructions from the literature, for the most part based on AWS data (Fig. S3). In the regridded dataset of (Nicolas and Bromwich, 2014), we observe a very low scaling at odds with the results from ERA5 or ice core records regardless of the calibration factor. This suggest that the decadal variability in the (Nicolas and Bromwich, 2014) reconstruction might not be of use for calibration purposes. If we compare to stack of AWS data (24 time series extracted from Berkeley Earth Surface Temperature (Rohde et al., 2013)), we obtain very similar properties than for

ERA5 at interannual and decadal time scales, suggesting that the impact of the discontinuity at the beginning of the satellite era might not affect strongly the decadal variability. It should be noted that the data from these AWS are most likely used to constrain ERA5 reanalysis product, and are as a result not independent. Nonetheless, this shows that the spectral properties of the ERA5 gridded product are relevant to calibrate our ice core record. For illustration purposes, we also indicate the spectrum of a single AWS at South Pole to compare with the results of (Clem et al., 2020). This spectral comparison also suggests that the spectral calibration is appropriate, and that difference between the assessed trend are not due to the isotope to temperature calibration of the stack.

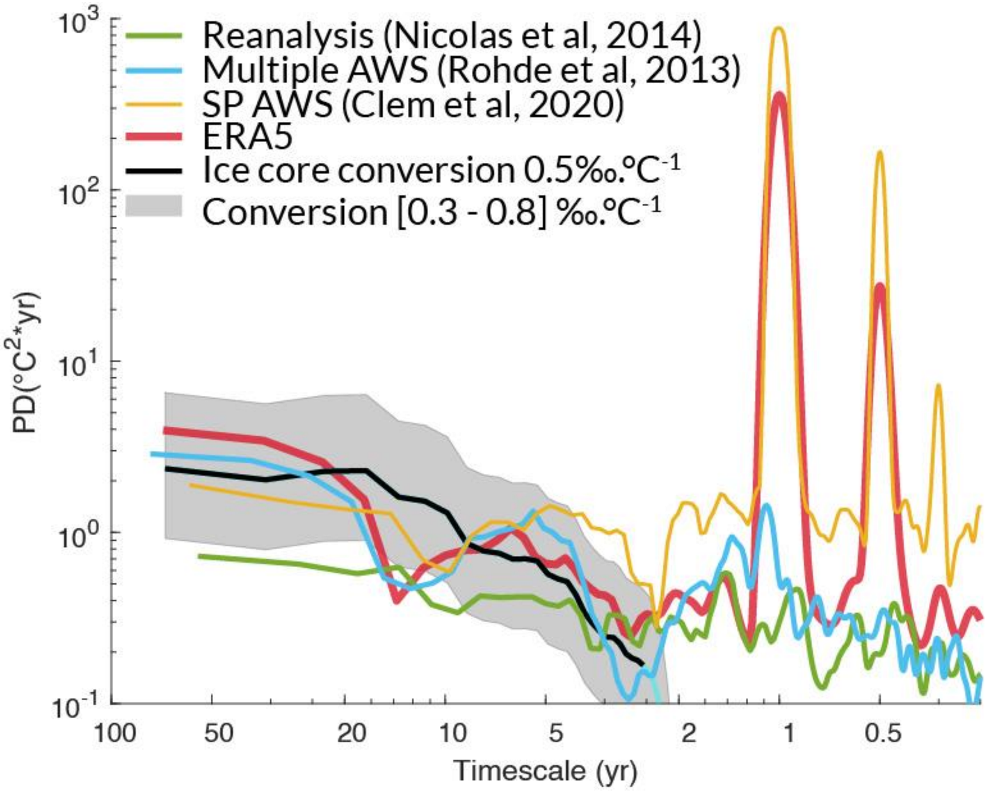

***Figure S3**: Spectral constraint of the isotope-temperature calibration: power spectral density of the reconstructed temperature for different values of $\Delta\delta$ 18O/ΔT between 1920 and 1990 compared to the spectrum of the ERA5 reanalysis outputs for the core location between 1951 and 2020 (the non-overlapping windows are set up to obtain the same length of time series with the largest number of cores; the results are insensitive to the window choice) as well as an ensemble of Antarctic temperature dataset from the literature: re-processed AWS from* (Nicolas and Bromwich, 2014), *multiple AWS data stacked together* (Rohde et al., 2013) *and the dataset from South Pole* (Clem et al., 2020).

7. CMIP simulations

We study the discrepancies between the anthropogenic warming predicted by CMIP5 and 6 ensemble models and the observations obtained from ice core records and ERA5. In the case of CMIP5, we use the eight P1000 simulations (see Table S5), which provide millennial runs of climate variability.

***Table S5**: CMIP5 simulations used in this study, all simulations cover at least the period from 1000 to 2005.*

Model	Country	Atm. grid spacing (lat x lon)	Reference
BCC-CSM1.1	China	2.8x2.8°	(Wu et al., 2013)
CCSM4	USA	0.9x1.25°	(Gent et al., 2011)
FGOALS-gl	China	2.8x2.8°	(Li et al., 2013)
GISS-E2-R-1	USA	2x2.5°	(Schmidt et al., 2014)
IPSL-CM5A-LR	France	1.9x3.8°	(Dufresne et al., 2013)
MIROC-ESM	Japan	2.8x2.8°	(Watanabe et al., 2010)
MPI-ESM	Germany	1.9x1.9°	(Roeckner et al., 2006)
MRI-CGCM3	Japan	1.12x1.13°	(Yukimoto et al., 2012)

For CMIP6, as the P1000 simulations are not available yet, we compare the ice core results to the historical simulations (r*i*p1f*, 131 simulations). For each simulation, we evaluate the trend of the current climate change similarly between 1950 and 2005 for the grid points of the ice cores.

***Table S6**: CMIP6 simulations used in this study, all simulations cover at least the period from 1850 to 2005.*

Model	Number of simulations	Country	Atm. grid spacing (lat x lon)	Reference
ACCESS-CM2	5	Australia	1.3x1.9°	(Bi et al., 2020)
ACCESS-ESM 1-5	40	Australia	1.2x1.9°	
BCC-CSM2-MR	4	China	1.1x1.1°	(Wu et al., 2019)
BCC-ESM1	4	China	2.8x2.8°	(Wu et al., 2020)
CAMS-CSM1-0	3	China	1.1x1.1°	(Rong et al., 2021)
CESM2-WACCM	3	USA	0.9x1.3°	(Liu et al., 2019)
CESM2	6	USA	0.9x1.3°	
CMCC-CM2-HR4	1	Italy	1.0x1.0°	(Cherchi et al., 2019)
CMCC-CM2-SR5	1	Italy	1.0x1.0°	
CMCC-ESM2	1	Italy	0.9x1.3°	(Lovato et al., 2022)
CanESM5	25	Canada	2.8x2.8°	(Swart et al., 2019)
FIO-ESM-2-0	3	China	0.9x1.3°	(Zhen-Ya et al., 2019)
MIROC-ES2H	1	Japan	1.3x1.3°	(Kawamiya et al., 2020)
MIROC-ES2L	31	Japan	2.8x2.8°	(Hajima et al., 2020)
MRI-ESM2-0	1	Japan	1.1x1.1°	(Yukimoto et al., 2019)
TaiESM1	2	Taiwan	0.9x1.3°	(Wang et al., 2021)

8. Definition of the persistence for typical climatic time series

In this section, we present the illustration of the meaning of the persistence compared to classical type of time series as often found to describe the climatic system. Namely, we evaluated the average value of the persistence of a time series modelled as a first-order auto-regressive process (AR(1)) characterised by a decay time τ (Fig. S4a), and for a time series modelled as a power law signal characterised with a scaling β (Fig. S4b). The persistence Theta is related to the temporal autocorrelation of the underlying signal. For example, in the case of a first-order autoregressive process with exponential autocorrelation, the persistence increases for increasing value of the underlying decay time τ (Fig S4a), and in the case of a fractional noise with power-law autocorrelation, it also increases for increasing values of the spectral scaling exponent β (Fig S4b).

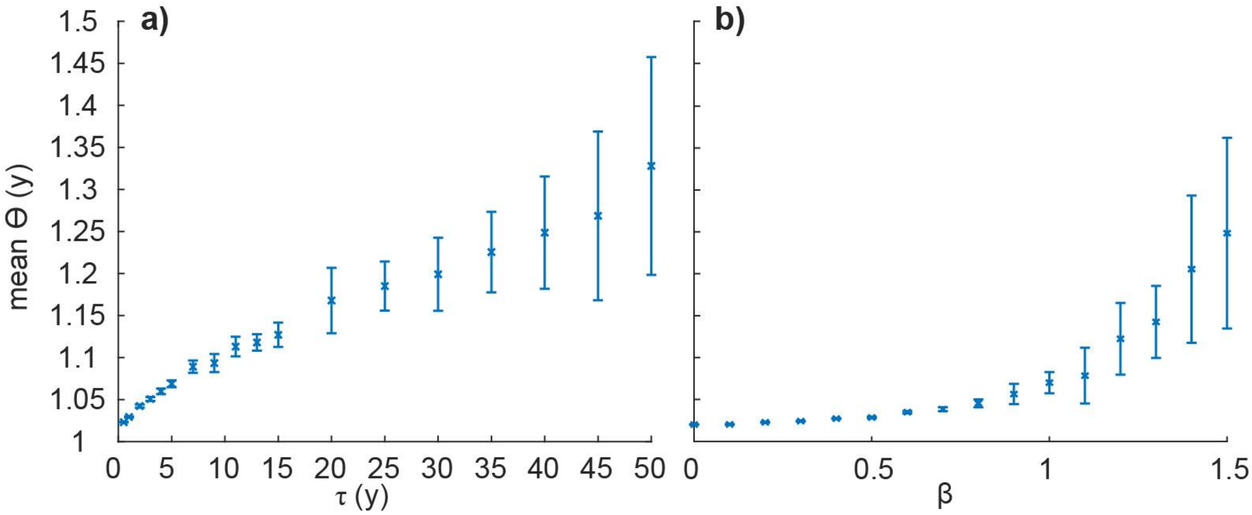

***Figure S4**: Average persistence for a) first-order auto-regressive process (AR1) and b) power law time series as a function of τ and β, respectively. a) The persistence was estimated from simulations of a first-order autoregressive process with increasing decay time τ, the vertical bars indicated the extent of the standard deviation around the mean of an ensemble of 1000 realisations of the process with given parameter. b) Same as a), but for a fractional noise process characterised by the spectral scaling exponent β; the fractional noise corresponds to fractional Gaussian noise when beta<1 and fractional Brownian motion when beta>1.*

SI references

Abram, N. J., McGregor, H. V, Tierney, J. E., Evans, M. N., McKay, N. P. and Kaufman, D. S.: Early onset of industrial-era warming across the oceans and continents, Nature, 536(7617), 411–418, 2016.

Bi, D., Dix, M., Marsland, S., O'farrell, S., Sullivan, A., Bodman, R., Law, R., Harman, I., Srbinovsky, J. and Rashid, H. A.: Configuration and spin-up of ACCESS-CM2, the new generation Australian community climate and earth system simulator coupled model, J. South. Hemisph. Earth Syst. Sci., 70(1), 225–251, 2020.

Casado, M., Ortega, P., Masson-Delmotte, V., Risi, C., Swingedouw, D., Daux, V., Genty, D., Maignan, F., Solomina, O., Vinther, B., Viovy, N. and Yiou, P.: Impact of precipitation intermittency on NAO-temperature signals in proxy records, Clim. Past, 9(2), 871–886, doi:10.5194/cp-9-871-2013, 2013.

Casado, M., Orsi, A. J. and Landais, A.: On the limits of climate reconstruction from water stable isotopes in polar ice cores, Past Glob. Chang. Mag., 25(3), 146–147, doi:10.22498/pages.25.3.146, 2017.

Casado, M., Landais, A., Picard, G., Münch, T., Laepple, T., Stenni, B., Dreossi, G., Ekaykin, A., Arnaud, L., Genthon, C., Touzeau, A., Masson-Delmotte, V. and Jouzel, J.: Archival processes of the water stable isotope signal in East Antarctic ice cores, Cryosph., 12(5), 1745–1766, doi:10.5194/tc-12-1745-2018, 2018.

Casado, M., Münch, T. and Laepple, T.: Climatic information archived in ice cores: impact of intermittency and diffusion on the recorded isotopic signal in Antarctica, Clim. Past, 16(4), 1581–1598, doi:10.5194/cp-16-1581-2020, 2020.
Cherchi, A., Fogli, P. G., Lovato, T., Peano, D., Iovino, D., Gualdi, S., Masina, S., Scoccimarro, E., Materia, S. and Bellucci, A.: Global mean climate and main patterns of variability in the CMCC-CM2 coupled model, J. Adv. Model. Earth Syst., 11(1), 185–209, 2019.
Christiansen, B. and Ljungqvist, F. C.: Challenges and perspectives for large-scale temperature reconstructions of the past two millennia, Rev. Geophys., 55(1), 40–96, doi:https://doi.org/10.1002/2016RG000521, 2017.
Clem, K. R., Fogt, R. L., Turner, J., Lintner, B. R., Marshall, G. J., Miller, J. R. and Renwick, J. A.: Record warming at the South Pole during the past three decades, Nat. Clim. Chang., 10(8), 762–770, 2020.
Dufresne, J.-L., Foujols, M.-A., Denvil, S., Caubel, A., Marti, O., Aumont, O., Balkanski, Y., Bekki, S., Bellenger, H. and Benshila, R.: Climate change projections using the IPSL-CM5 Earth System Model: from CMIP3 to CMIP5, Clim. Dyn., 40(9), 2123–2165, 2013.
Gent, P. R., Danabasoglu, G., Donner, L. J., Holland, M. M., Hunke, E. C., Jayne, S. R., Lawrence, D. M., Neale, R. B., Rasch, P. J. and Vertenstein, M.: The community climate system model version 4, J. Clim., 24(19), 4973–4991, 2011.
Gkinis, V., Holme, C., Kahle, E. C., Stevens, M. C., Steig, E. J. and Vinther, B. M.: Numerical experiments on firn isotope diffusion with the Community Firn Model, J. Glaciol., 67(263), 450–472, 2021.
Goosse, H., Renssen, H., Timmermann, A. and Bradley, R. S.: Internal and forced climate variability during the last millennium: a model-data comparison using ensemble simulations, Quat. Sci. Rev., 24(12–13), 1345–1360, 2005.
Guillevic, M., Bazin, L., Landais, A., Kindler, P., Orsi, A., Masson-Delmotte, V., Blunier, T., Buchardt, S. L., Capron, E. and Leuenberger, M.: Spatial gradients of temperature, accumulation and $δ$ 18 O-ice in Greenland over a series of Dansgaard–Oeschger events, Clim. Past, 9(3), 1029–1051, 2013.
Hajima, T., Watanabe, M., Yamamoto, A., Tatebe, H., Noguchi, M. A., Abe, M., Ohgaito, R., Ito, A., Yamazaki, D. and Okajima, H.: Development of the MIROC-ES2L Earth system model and the evaluation of biogeochemical processes and feedbacks, Geosci. Model Dev., 13(5), 2197–2244, 2020.
Huybers, P. and Curry, W.: Links between annual, Milankovitch and continuum temperature variability, Nature, 441(7091), 329–332, 2006.
Kawamiya, M., Hajima, T., Tachiiri, K., Watanabe, S. and Yokohata, T.: Two decades of Earth system modeling with an emphasis on Model for Interdisciplinary Research on Climate (MIROC), Prog. Earth Planet. Sci., 7(1), 1–13, 2020.
Küttel, M., Steig, E. J., Ding, Q., Monaghan, A. J. and Battisti, D. S.: Seasonal climate information preserved in West Antarctic ice core water isotopes: relationships to temperature, large-scale circulation, and sea ice, Clim. Dyn., 39(7), 1841–1857, doi:10.1007/s00382-012-1460-7, 2012.
Laepple, T., Münch, T., Casado, M., Hoerhold, M., Landais, A. and Kipfstuhl, S.: On the similarity and apparent cycles of isotopic variations in East Antarctic snow pits, Cryosph., 12(1), 169–187, doi:10.5194/tc-12-169-2018, 2018.
Landais, A., Casado, M., Prié, F., Magand, O., Arnaud, L., Ekaykin, A., Petit, J.-R., Picard, G., Fily, M. and Minster, B.: Surface studies of water isotopes in Antarctica for quantitative

interpretation of deep ice core data, Comptes Rendus Geosci., 2017.
Li, L., Lin, P., Yu, Y., Wang, B., Zhou, T., Liu, L., Liu, J., Bao, Q., Xu, S. and Huang, W.: The flexible global ocean-atmosphere-land system model, Grid-point Version 2: FGOALS-g2, Adv. Atmos. Sci., 30(3), 543–560, 2013.
Liu, S.-M., Chen, Y.-H., Rao, J., Cao, C., Li, S.-Y., Ma, M.-H. and Wang, Y.-B.: Parallel comparison of major sudden stratospheric warming events in CESM1-WACCM and CESM2-WACCM, Atmosphere (Basel)., 10(11), 679, 2019.
Lovato, T., Peano, D., Butenschön, M., Materia, S., Iovino, D., Scoccimarro, E., Fogli, P. G., Cherchi, A., Bellucci, A. and Gualdi, S.: CMIP6 Simulations With the CMCC Earth System Model (CMCC-ESM2), J. Adv. Model. Earth Syst., 14(3), e2021MS002814, 2022.
Lovejoy, S. and Schertzer, D.: The weather and climate: emergent laws and multifractal cascades, Cambridge University Press., 2013.
Masson-Delmotte, V., Hou, S., Ekaykin, A., Jouzel, J., Aristarain, A., Bernardo, R. T., Bromwich, D., Cattani, O., Delmotte, M., Falourd, S., Frezzotti, M., Gallée, H., Genoni, L., Isaksson, E., Landais, A., Helsen, M. M., Hoffmann, G., Lopez, J., Morgan, V., Motoyama, H., Noone, D., Oerter, H., Petit, J. R., Royer, A., Uemura, R., Schmidt, G. A., Schlosser, E., Simões, J. C., Steig, E. J., Stenni, B., Stievenard, M., van den Broeke, M. R., van de Wal, R. S. W., van de Berg, W. J., Vimeux, F. and White, J. W. C.: A Review of Antarctic Surface Snow Isotopic Composition: Observations, Atmospheric Circulation, and Isotopic Modeling*, J. Clim., 21(13), 3359–3387, doi:10.1175/2007JCLI2139.1, 2008.
Münch, T. and Laepple, T.: What climate signal is contained in decadal-to centennial-scale isotope variations from Antarctic ice cores?, Clim. Past, 14(12), 2053–2070, 2018.
Nicolas, J. P. and Bromwich, D. H.: New Reconstruction of Antarctic Near-Surface Temperatures: Multidecadal Trends and Reliability of Global Reanalyses, J. Clim., 27(21), 8070–8093, doi:doi:10.1175/JCLI-D-13-00733.1, 2014.
Osborn, T. J. and Briffa, K. R.: The real color of climate change?, Science (80-.)., 306(5696), 621–622, 2004.
Percival, D. B. and Walden, A. T.: Spectral analysis for physical applications, cambridge university press., 1993.
Rodionov, S. N.: The problem of red noise in climate regime shift detection, Geophys. Res. Lett., 31, L12707, 2006.
Roeckner, E., Brokopf, R., Esch, M., Giorgetta, M. A., Hagemann, S., Kornblueh, L., Manzini, E., Schlese, U. and Schulzweida, U.: Sensitivity of simulated climate to horizontal and vertical resolution in the ECHAM5 atmosphere model, J. Clim., 19(16), 3771–3791, 2006.
Rohde, R., Muller, R., Jacobsen, R., Perlmutter, S., Rosenfeld, A., Wurtele, J., Curry, J., Wickhams, C. and Mosher, S.: Berkeley Earth Temperature Averaging Process, Geoinfor. Geostat.-An Overview, 1, 2, Geoinformatics Geostatistics An Overv., 1(2), 20–100, 2013.
Rong, X., Li, J., Chen, H., Su, J., Hua, L., Zhang, Z. and Xin, Y.: The CMIP6 historical simulation datasets produced by the climate system model CAMS-CSM, Adv. Atmos. Sci., 38(2), 285–295, 2021.
Schmidt, G. A., Kelley, M., Nazarenko, L., Ruedy, R., Russell, G. L., Aleinov, I., Bauer, M., Bauer, S. E., Bhat, M. K. and Bleck, R.: Configuration and assessment of the GISS ModelE2 contributions to the CMIP5 archive, J. Adv. Model. Earth Syst., 6(1), 141–184, 2014.
Stenni, B., Curran, M. A. J., Abram, N., Orsi, A., Goursaud, S., Masson-Delmotte, V., Neukom, R., Goosse, H., Divine, D. and Van Ommen, T.: Antarctic climate variability on regional and continental scales over the last 2000 years, Clim. Past, 13, 1609–1634, 2017.

Von Storch, H., Zorita, E., Jones, J. M., Dimitriev, Y., González-Rouco, F. and Tett, S. F. B.: Reconstructing past climate from noisy data, Science (80-.)., 306(5696), 679–682, 2004.
Swart, N. C., Cole, J. N. S., Kharin, V. V, Lazare, M., Scinocca, J. F., Gillett, N. P., Anstey, J., Arora, V., Christian, J. R. and Hanna, S.: The Canadian earth system model version 5 (CanESM5. 0.3), Geosci. Model Dev., 12(11), 4823–4873, 2019.
Touzeau, A., Landais, A., Stenni, B., Uemura, R., Fukui, K., Fujita, S., Guilbaud, S., Ekaykin, A., Casado, M., Barkan, E., Luz, B., Magand, O., Teste, G., Le Meur, E., Baroni, M., Savarino, J., Bourgeois, I. and Risi, C.: Acquisition of isotopic composition for surface snow in East Antarctica and the links to climatic parameters, Cryosph., 10(2), 837–852, doi:10.5194/tc-10-837-2016, 2016.
Wang, Y., Hsu, H., Chen, C., Tseng, W., Hsu, P., Lin, C., Chen, Y., Jiang, L., Lee, Y. and Liang, H.: Performance of the taiwan earth system model in simulating climate variability compared with observations and CMIP6 model simulations, J. Adv. Model. Earth Syst., 13(7), e2020MS002353, 2021.
Watanabe, M., Suzuki, T., O'ishi, R., Komuro, Y., Watanabe, S., Emori, S., Takemura, T., Chikira, M., Ogura, T. and Sekiguchi, M.: Improved climate simulation by MIROC5: mean states, variability, and climate sensitivity, J. Clim., 23(23), 6312–6335, 2010.
Werner, M., Jouzel, J., Masson-Delmotte, V. and Lohmann, G.: Reconciling glacial Antarctic water stable isotopes with ice sheet topography and the isotopic paleothermometer, Nat. Commun., 9(1), 3537, doi:10.1038/s41467-018-05430-y, 2018.
Wu, T., Li, W., Ji, J., Xin, X., Li, L., Wang, Z., Zhang, Y., Li, J., Zhang, F. and Wei, M.: Global carbon budgets simulated by the Beijing Climate Center Climate System Model for the last century, J. Geophys. Res. Atmos., 118(10), 4326–4347, 2013.
Wu, T., Lu, Y., Fang, Y., Xin, X., Li, L., Li, W., Jie, W., Zhang, J., Liu, Y. and Zhang, L.: The Beijing Climate Center climate system model (BCC-CSM): the main progress from CMIP5 to CMIP6, Geosci. Model Dev., 12(4), 1573–1600, 2019.
Wu, T., Zhang, F., Zhang, J., Jie, W., Zhang, Y., Wu, F., Li, L., Yan, J., Liu, X. and Lu, X.: Beijing Climate Center Earth System Model version 1 (BCC-ESM1): model description and evaluation of aerosol simulations, Geosci. Model Dev., 13(3), 977–1005, 2020.
Yukimoto, S., Adachi, Y., Hosaka, M., Sakami, T., Yoshimura, H., Hirabara, M., Tanaka, T. Y., Shindo, E., Tsujino, H. and Deushi, M.: A new global climate model of the Meteorological Research Institute: MRI-CGCM3—Model description and basic performance—, J. Meteorol. Soc. Japan. Ser. II, 90, 23–64, 2012.
Yukimoto, S., Kawai, H., Koshiro, T., Oshima, N., Yoshida, K., Urakawa, S., Tsujino, H., Deushi, M., Tanaka, T. and Hosaka, M.: The Meteorological Research Institute Earth System Model version 2.0, MRI-ESM2. 0: Description and basic evaluation of the physical component, J. Meteorol. Soc. Japan. Ser. II, 2019.
Zhen-Ya, S., Ying, B. A. O. and Fang-Li, Q.: Introduction of FIO-ESM v2. 0 and its participation plan in CMIP6 experiments, Adv. Clim. Chang. Res., 15(5), 558, 2019.
Zhu, F., Emile-Geay, J., McKay, N. P., Hakim, G. J., Khider, D., Ault, T. R., Steig, E. J., Dee, S. and Kirchner, J. W.: Climate models can correctly simulate the continuum of global-average temperature variability, Proc. Natl. Acad. Sci., 116(18), 8728–8733, 2019.